physica status solidi pss a
www.pss-a.com

Check for updates

High Power Laser-Driven Ce^{3+}-Doped Yttrium Aluminum Garnet Phosphor Incorporated Sapphire Disc for Outstanding White Light Conversion Efficiency

*Kanika Garima Kedawat, Pratima Kundu, Ritu Srivastava, Jagjeevan K. Jain, Hem C. Kandpal, and Bipin Kumar Gupta**

A facile synthesis method for the development of $Y_{3-x}Al_5O_{12}:xCe^{3+}$ ($x = 0.03$–0.24) yellow phosphor via an auto-combustion method and fabrication of phosphor-incorporated sapphire disc (PISD) of various dimensions is reported. The photoluminescence (PL) intensity for the optimized concentration of Ce^{3+}-doped yttrium aluminum garnet (YAG) phosphor is recorded at 550 nm wavelength under the excitation wavelength of 445 nm from a high power blue laser diode. The developed PISD exhibits high stability and luminescence. The blue laser diode is a promising candidate to revolutionize the luminous intensity of the white light by several orders of magnitude as compared with the existing blue light-emitting diodes. This emerging technology has an extremely bright future with endless uses of tunable power of the laser that controls the intensity of the emitted white light. Hence, this new approach provides a paradigm shift to produce highly efficient white light based on PISD integrated with blue laser diode as compared with the conventional technology. Moreover, such configurations allow more styling and packaging flexibility that reduces the overall size of the fabricated unit and makes it favorable for various lighting applications.

1. Introduction

Solid-state lighting (SSL) devices have become a paragon source of generating light and are growing exponentially for various lighting applications, namely, automotive lighting, indoor and outdoor lighting, medical applications, and also modern lifestyle products.[1,2] The invention of efficient blue light-emitting diodes (LEDs) using indium gallium nitiride (InGaN) enabling bright and energy-saving white light sources has potentially reignited research for white LEDs (WLEDs) applications.[2,3] WLEDs are good candidates as next-generation SSL devices and are capable of replacing incandescent and fluorescent lamps due to their outstanding properties, such as low power consumption, huge energy saving, high quantum efficiency, fast response, long lifetime, high luminance, and better compactness.[4–7] The phosphor-converted WLEDs are the potential candidate for remarkable reduction in global energy consumption of lighting.

In general, there are several approaches to generate high intense white light using the combination of blue LEDs with yellow phosphor ($Y_3Al_5O_{12}:Ce^{3+}$; named as YAG:Ce) is one of them.[2–4,8] The mechanism of WLEDs is based upon the optical pumping of the integrated yellow emitting luminophores through blue light, produced from InGaN LEDs via electroluminescence phenomenon, whereas under the excitation of blue LEDs, YAG:Ce phosphor emits a broad spectrum from 500 to 650 nm, due to the 5d-4f transition of Ce^{3+} ion. Yttrium aluminum garnet ($Y_3Al_5O_{12}$; YAG) is a synthetic crystalline material of the garnet group and possesses many interesting properties such as excellent thermal conductivity, high mechanical strength, and good temperature as well as radiation resistance.[8–10] Therefore, the high efficiency of YAG:Ce phosphor facilitates a better luminescence performance in WLEDs, as YAG exhibits high luminescence quantum yield, short decay lifetime, and extended thermal stability. These important key factors are responsible for its wide acceptance as a commercial phosphor for WLEDs.

However, this strategy based on YAG:Ce phosphors in LEDs suffers critical problems associated with thermal quenching in luminescence due to the higher operating current of LEDs, low color-rendering index, and high color-temperature. The increase in the operating current augments the temperature, which in turn decreases LEDs efficiency, further altering the device color output.[11] Moreover, the YAG:Ce-based blue LEDs have some drawbacks related to the effect of temperature that are produced from the LEDs on phosphor, which results in decreases in the efficiency and a possible shift in emission wavelength of yellow phosphor that obstructed their use in versatile applications. Ultimately, the efficiency of WLEDs decreases and

Dr. K. G. Kedawat, P. Kundu, Dr. R. Srivastava, Dr. B. K. Gupta
Photonic Materials Metrology Sub Division
Advanced Materials and Device Metrology Division
CSIR-National Physical Laboratory
Dr K. S. Krishnan Road, New Delhi 110012, India
E-mail: bipinbhu@yahoo.com; guptabgupta@nplindia.org

Dr. J. K. Jain, Dr. H. C. Kandpal
Fiem Industries Ltd.
Plot No. 1915, Rai Industrial Estate, Phase 5, Sonepat 131029, Haryana, India

The ORCID identification number(s) for the author(s) of this article can be found under https://doi.org/10.1002/pssa.201900110.

DOI: 10.1002/pssa.201900110

it is a challenging task to employ YAG:Ce phosphor on high power blue LEDs. In comparison with blue LEDs, blue laser diodes can be a better alternative source to resolve the issues created by the LEDs. Thus, the blue laser diode could be used as a next light source that would revolutionize the lighting technology especially in automotive lighting applications.[12,13] In addition, the color stability of laser can be maintained because of the characteristic behavior of the output power. The external quantum efficiency (EQE) of laser diodes also increases linearly as a function of operating current. Furthermore, the thermal stability of YAG:Ce phosphor is also required with blue laser diodes for the generation of white light. It is essential that the use of organic resin such as epoxy and silicone polycrystalline phosphor powder with YAG:Ce phosphor is required for designing composite disc.[13] This composite disc is placed in front of the blue laser diodes for increasing the luminous efficacy and power intensity, thereby enhancing the life and performance of white light. However, the use of YAG:Ce composite disc with blue laser diodes for white light generation to be used widely in displays, lamps, light fidelity, and automotive lighting, which has yet to be investigated in details.[12–14] There are several efforts that have been employed for the synthesis of YAG:Ce phosphor powder using different techniques such as co-precipitation, sol–gel, combustion, and spray pyrolysis to obtain high crystallinity, large luminous power, and small particle size.[8] This type of laser diodes is a milestone for the development of today's omnipresent white lights. Therefore, blue laser diode and YAG:Ce phosphor could be the best complement to each other to design an efficient laser-induced white light for future generation applications. In this study, a new strategy has been defined to fabricate a light-weight phosphor-incorporated sapphire disc (PISD) geometry by incorporating YAG:Ce phosphor in epoxy resin and sandwiched it in between two sapphire discs to produce highly efficient luminescence with better thermal stability. The advantage of the sapphire disc is to dissipate the overheating of phosphor caused by the high power laser. The combined arrangement of PISD with a blue laser diode for the generation of outstanding white light could be used to fulfill the current demand of several lighting industries especially in automotive lighting. To the best of our knowledge, such light-weight PISD geometry with the proposed configuration has not been reported so far.

2. Results and Discussion

2.1. Crystalline Structure

The X-ray diffraction (XRD) study was performed to analyze the gross average structure and confirm the phase purity of YAG:Ce phosphor synthesized by the auto-combustion method. **Figure 1**a shows the XRD pattern of YAG:Ce (6 mol%, optimized sample, details described in the Experimental Section) phosphor. The XRD result reveals that the as-synthesized YAG:Ce phosphor exhibits well-defined peaks of pure YAG phase and has a garnet

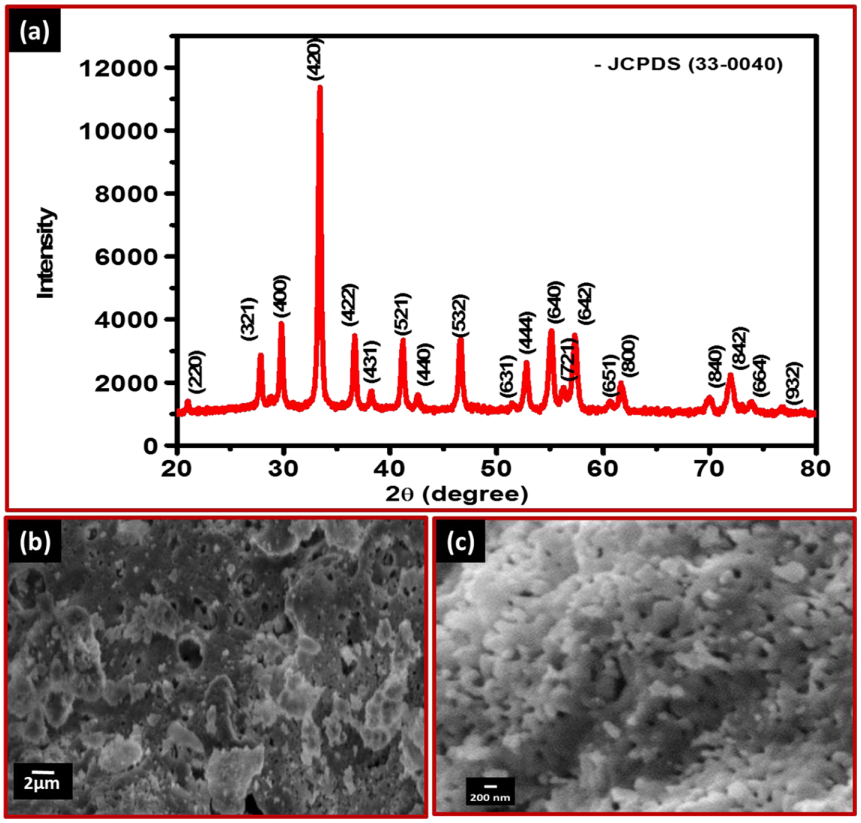

Figure 1. a) XRD pattern of YAG:Ce (6%) phosphor, XRD pattern is indexed using JCPDS Card No.33-0040. b) SEM micrograph of YAG:Ce (6%) phosphors. c) Magnified view of YAG:Ce (6%) phosphors.

structure, which is closely matched with the JCPDS Card No. 33-0040. This shows that the dopant ions (Ce^{3+}) completely occupy the place of Y in the YAG host lattice during the formation of the YAG:Ce phase. Any additional phase has not been observed such as the orthorhombic perovskite phase of YAP ($Y_4Al_2O_9$) or the monocline phase of YAM ($YAlO_3$). A YAG:Ce crystal has a cubic phase that belongs to the Ia^3d space group with the lattice parameters $a = b = c = (12.01063 \pm 0.00046)$ Å, which are in close approximation to the standard values of these parameters, i.e., $a = b = c = 12.00890$ Å, calculated using the unit cell refinement software.[16]

2.2. Surface Topography

Surface morphology of as-synthesized YAG:Ce phosphor was studied using scanning electron microscopy (SEM). Figure 1b, c represents the SEM image and its magnified view of as synthesized YAG:Ce (6 mol%) phosphor, respectively. The images show the hierarchical structure of YAG:Ce phosphor having an average particle size of $\approx 200 \pm 10$ nm. The magnified view reveals that these agglomerated particles are randomly distributed throughout the surface area.

2.3. Photoluminescence Spectroscopy

The spectroscopic properties of YAG:Ce phosphor were investigated by using photoluminescence (PL) and time-resolved photoluminescence (TRPL) spectroscopic techniques. A xenon lamp was used as a source of excitation for PL while a pulsed xenon lamp with a single photon sensitive detector was used for TRPL. The optimization of the concentration of Ce^{3+} ion in the YAG host lattice is desired for highest luminescence intensity. The various concentrations of Ce^{3+} ion (2, 4, 6, and 8 mol%) were doped in the YAG host lattice, and their corresponding PL analysis was performed to obtain the optimized concentrations shown in Supporting Information (Figure S1, Supporting Information). The PL results reveal that the 6 mol% of Ce^{3+} ion is the optimum doping concentration value for the YAG host lattice ($Y_{3-x}Al_5O_{12}$:xCe^{3+}; $x = 0.18$). In addition, it has been observed that the PL emission intensity increases as the concentration of Ce^{3+} ion increases up to $x = 0.18$ (6 mol%) and decreases beyond the optimum concentration ($x > 0.18$). The luminescence quenching occurs beyond the optimum concentration of Ce ($x > 0.18$), and it may be due to the presence of excess of Ce^{3+} ions. In high doping concentrations beyond 6 mol%, the nonradiative rate exceeds the energy transfer rate due to the less distance between two Ce ions, where these mutually interact with each other easily by an electric multipolar process. The absorbed wavelength photons quickly drift Ce^{3+} ions toward the host lattice, where the luminescence reduces and decrease the probabilities of the radiative transitions of Ce^{3+} ions. Furthermore, the excited state gets trapped in an energy sink with a high nonradiative deactivation rate, which ultimately leads to quenching in of fluorescence.[15] However, for the concentration of Ce^{3+} ion $\leq$6 mol%, the distance between two Ce^{3+} ions will be considerably large, where both Ce^{3+} ions act as separate luminescent centers and produce high luminescence without any obstruction. Thus, the distance between two Ce^{3+} ions in the host lattice is a key parameter to avoid luminescence quenching, which can be easily controlled by optimum substitution of dopants in the host lattice. Therefore, the optimum doping concentration is a very important parameter while designing a rare earth–doped phosphor to obtain highly efficient luminescence.[16] Furthermore, the critical distance between two Ce^{3+} ions using Dexter's theory has also been estimated. According to Dexter's theory, the value of critical distance R_c can be calculated via the following Equation (1)

$$R_c = 2(3V/4\pi x_c N)^{1/3} \quad (1)$$

where V represents the unit cell, x_c is the critical quenching concentration, and N is the number of Ce^{3+} ions per unit cell. The calculated critical distance (R_c) between the two Ce^{3+} ions is 9.14 Å by adopting the value of $V = 1731.847$ Å^3, $N = 24$, and $x_c = 0.18$.

The energy level diagram shows the transition states of Ce-doped YAG phosphor when excited with the blue laser diode, as shown in Supporting Information (Figure S2, Supporting Information). These transitions of dopant Ce^{3+} in the YAG host lattice are consistent with the analysis of luminescent spectra of YAG:Ce at different doping concentrations of Ce (Figure S1, Supporting Information). The excitation and emission spectra of optimized $Y_{2.82}Al_5O_{12}$:0.18 Ce^{3+} phosphor are shown in the **Figure 2**a. The inset of Figure 2a shows the optical image of as-synthesized $Y_{2.82}Al_5O_{12}$:0.18 Ce^{3+} phosphor under the day light. The excitation spectrum of $Y_{2.82}Al_5O_{12}$:0.18 Ce^{3+} phosphor has been recorded at room temperature upon fixed emission wavelength of 550 nm. The spectrum exhibits two peaks; a less intense and a high intense peak appears in the ranges from 320–360 and 390–520 nm centered at 345 and 450 nm, respectively. The high intense excitation peak of $Y_{2.82}Al_5O_{12}$:0.18 Ce^{3+} phosphor occurs due to the transitions in ions from the ground state $^2F_{5/2}$ to the upper 5d state, which is further split by the crystal field into two different states $^2D_{3/2}$ and $^2D_{5/2}$, as shown in Figure S2, Supporting Information, whereas the less intense peak that appears at 345 nm (3.59 eV) wavelength is due to the transitions to the upper 5d state as shown in Figure 2a. The PL emission spectrum has been taken under the excitation wavelength of 450 nm via a xenon lamp, which acts as a source of excitation. An intense asymmetric broad emission spectrum was observed from 475 to 700 nm with the centered peak at 550 nm wavelength, which is the sum of the two transitions from the phonon-relaxed 5d states $^2A_{1\{g\}}$ to the spin-orbit coupling split levels of the ground state $^2F_{7/2}$ and $^2F_{5/2}$.[17–19] Figure 2b shows the chromaticity diagram of Commission Internationale de l'Elcairage (CIE) color coordinates estimated from the PL emission spectrum of $Y_{2.82}Al_5O_{12}$:0.18 Ce^{3+} phosphor, which are $X = 0.4488$ and $Y = 0.5331$. The internal quantum yield is evaluated by the integrated fraction of the luminous flux and radiant flux, which are measured with the standard method using following equation

$$\eta = \frac{\text{number of photons emitted}}{\text{number of photons absorbed}} \quad (2)$$

$$\eta = \frac{L_{\text{sample}}}{E_{\text{reference}} - E_{\text{sample}}} \quad (3)$$

where η represents internal quantum yield, L_{sample} the emission intensity, $E_{\text{reference}}$ and E_{sample} the intensities of the excitation

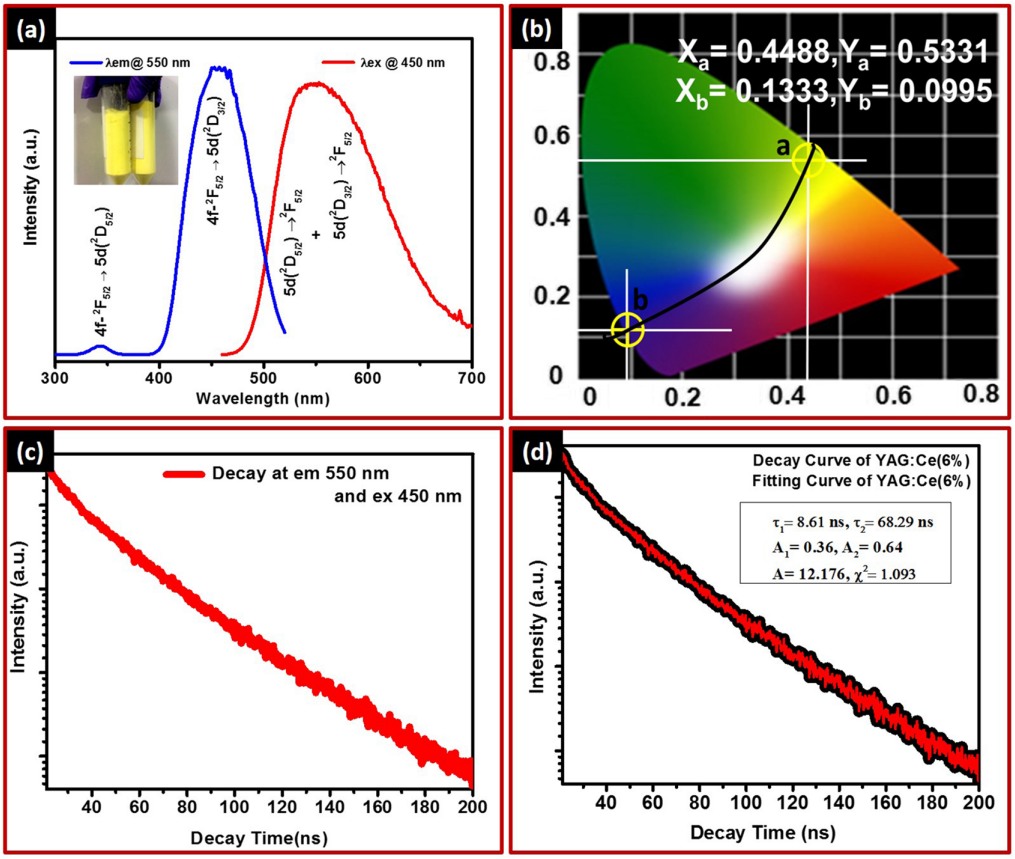

Figure 2. a) Normalized excitation and emission spectra of YAG:Ce (6%) phosphor. The inset exhibits yellow body color of as-synthesized phosphor under ordinary light. b) CIE coordinates of YAG:Ce (6%) phosphors and blue laser. c) TRPL spectrum of YAG:Ce (6%) phosphors. d) The fitting curve and corresponding parameters for YAG:Ce (6%) phosphor.

light not absorbed by the reference and the sample, respectively. The estimated internal quantum yield of $Y_{2.82}Al_5O_{12}$:0.18 Ce^{3+} phosphor is 83%, which is much more than the commercially available yellow phosphor (internal quantum yield ≈71%). Furthermore, we have also compared the PL spectra of phosphors synthesized in our laboratory with the commercially available yellow phosphor, and results are stated in Figure S3, Supporting Information.

Figure 2c represents the TRPL spectrum of $Y_{2.82}Al_5O_{12}$:0.18 Ce^{3+} phosphor. TPRL is a nondestructive and a powerful technique to determine the excitation lifetime of phosphors that defines the performance of luminescent materials and its suitable applications. The TRPL decay time was recorded at room temperature for the Ce^{3+} transitions at 550 nm emission upon excitation wavelength of 450 nm. The TRPL result reveals that the $Y_{2.82}Al_5O_{12}$:0.18 Ce^{3+} phosphor decay time is in the range of nanoseconds. Figure 2d shows the fitting curve of experimentally observed decay profile of the $Y_{2.82}Al_5O_{12}$:0.18 Ce^{3+} phosphor. Furthermore, the generated parameters of the fitting decay profile of $Y_{2.82}Al_5O_{12}$:0.18 Ce^{3+} phosphor is shown in the inset of Figure 2d. All the decay curves cannot be fitted by single exponential decay, which implies that multiple processes in addition to the radiative transition might have been involved during the decay of emission. The lifetime data of $Y_{2.82}Al_5O_{12}$:0.18 Ce^{3+} phosphor were well fitted to a double-exponential function as described by Equation (4) below

$$I(t) = A_1 \exp(-t/\tau_1) + A_2 \exp(-t/\tau_2) \quad (4)$$

where τ_1 and τ_2 are the decay lifetimes of the luminescence, and A_1 and A_2 are the weighting parameters. The parameters generated from the fitting are listed in Figure 2d. The obtained lifetimes for the phosphor are $\tau_1 = 8.61$ ns and $\tau_2 = 68.29$ ns. The lifetime results have shown second-order exponential decay, which has good consistency with earlier reported results.[20] The two ground states of $4f^1$ configuration ($^2F_{7/2}$ and $^2F_{5/2}$) depends upon the orbital and spin momenta of the electron whether they are parallel or anti-parallel. As the 5d-4f transitions belong to an electric dipole, the emission has a very short lifetime. Moreover, during 5d-4f transition in Ce^{3+} ion, spin selection is not appropriate and it is parity allowed. As a result, the emission transition at 540 nm is completely allowed one, and a strong luminescence intensity is observed with a very short lifetime in the order of nanoseconds.

After characterizing the $Y_{2.82}Al_5O_{12}$:0.18 Ce^{3+} phosphor, we have fabricated a light weight and thermally stable PISD by fusing $Y_{2.82}Al_5O_{12}$:0.18 Ce^{3+} phosphor into an epoxy resin, which is further sandwiched between two sapphire discs to produce

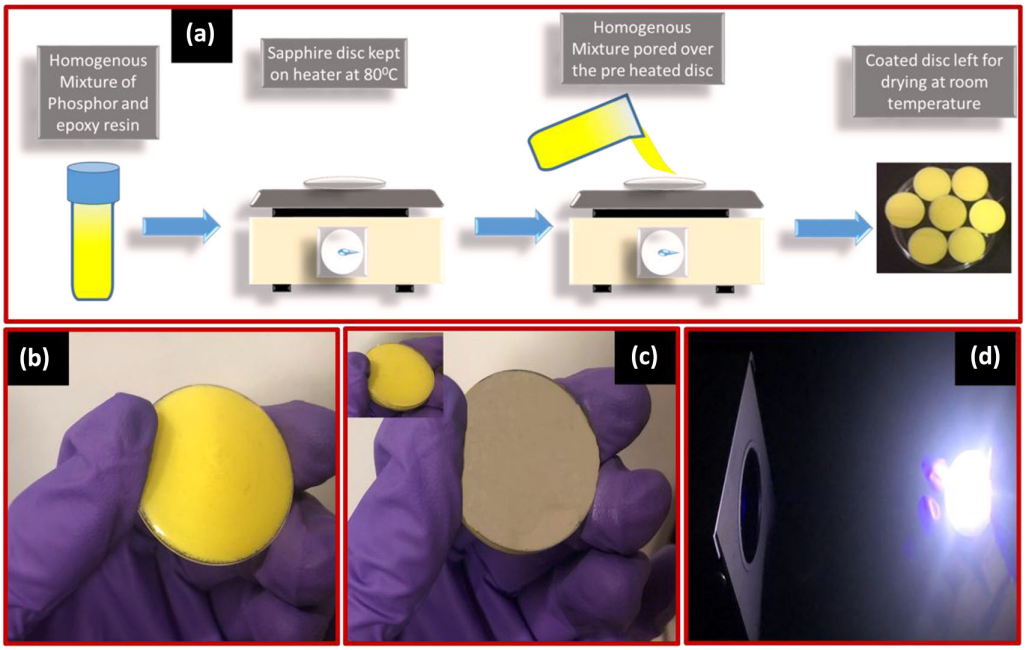

Figure 3. a) Schematic diagram of disc fabrication. b) Fabricated disc for transmission mode. c) Fabricated disc for reflection mode. d) Laser-induced white light for consistency check.

highly efficient white light; the schematic of the PISD fabrication is shown in **Figure 3**a. The sapphire discs are used to protect the phosphor-epoxy layer because this layer alone is not capable to withstand against the maximum local irradiance produced by the laser beam (≈40 °C). Figure 3b,c represents the optical image of PISD for transmission and reflection modes, respectively, under the day light. There is a difference in PISD used in transmission mode than the PISD used in the reflection mode. In the transmission mode, both surfaces, i.e, top and bottom of PISD are protected with transparent sapphire discs, while the reflection mode PISD has its bottom sapphire disc coated with aluminum (thickness of 40 nm) using the thermal evaporation technique; the optical image is shown in the inset of Figure 3c, whereas the top sapphire disc that is exposed to the laser beam remains uncoated. Since, sapphire is extremely chemically stable at high temperatures (melting point, 2040 °C) with the largest energy gap of ≈9.1 eV, which allows excellent transmission with the very less absorption from 0.25 to 5.00 μ. Mostly, sapphire is used for stringent optical applications, which mainly involves exposure to high stresses and harsh environments.[21] The stability of a sapphire disc as a protective layer is experimentally verified when the phosphor-epoxy layer is directly exposed to the laser beam; the disc sustained only for 1 min and then got burned, as shown in **Figure 4**. On the other hand, when PISD is exposed to the intense laser beam (≈40 °C), it stands against the same blue laser for several hours without any damage or burn on the surface. Hence, it passes the thermal stability test that is done in an in-house setup shown in **Figure 5**. The inset of Figure 5b shows an optical image of uneffected PISD. Furthermore, the thermal luminescence at different temperatures has been measured using the in-house setup, and the result is shown in **Figure 6**. The obtained result depicts that PISD is highly stable and has

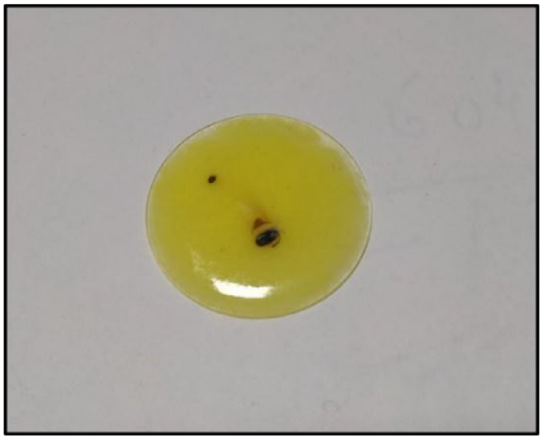

Figure 4. Phosphor-epoxy layer without integrating sapphire. The optical image clearly exhibits burning of the sample after exposure with blue laser (0.8 W) beam.

uniform PL intensity at all temperatures (20, 40, 60, 80, and 100 °C). The major advantage in the fabrication PISD was not only to improve the stability of disc but also allowed very good results in terms of the uniformity of the blue laser beam and provides a constant thickness of phosphor throughout the circular disc area.

2.4. Transmission versus Reflection Modes

To explore the feasibility of blue laser-induced white light using PISD for headlight geometry in automotive applications, various

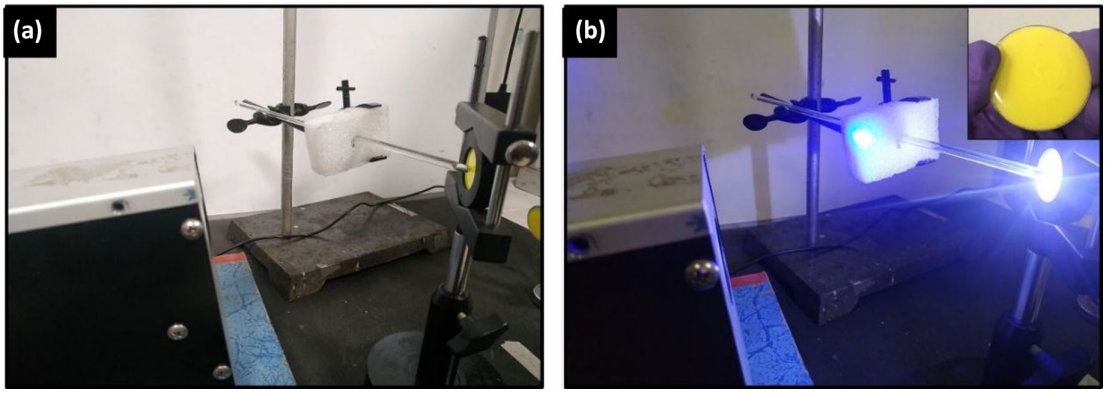

Figure 5. a) Setup to examine the thermal stability of as-synthesized phosphor PISD and b) measuring the thermal stability, where inset of (b) shows the PISD after several hours exposure to the high intense laser beam.

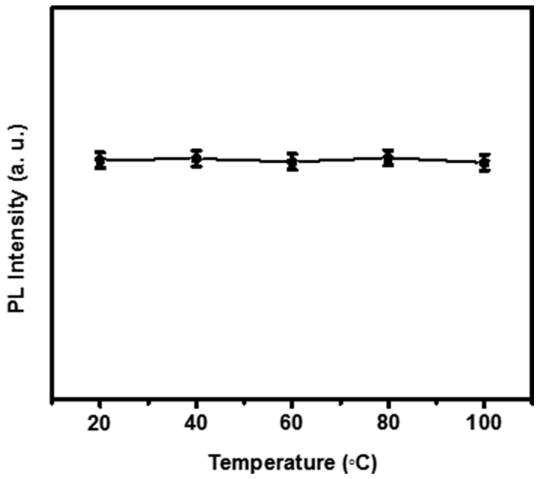

Figure 6. PL spectra of PISD at different temperatures; 20, 40, 60, 80, and 100 °C to explore the thermal luminescence characteristics.

modes with different PISDs are proposed depending upon the arrangement geometry of PISD with respect to the blue laser diode: 1) transmission mode and 2) reflection mode, where the laser was kept fixed at one place and the arrangement of other objects, such as PISD, reflector may vary.

2.4.1. Transmission Mode

White light generation in the transmission mode had a simple arrangement. During the transmission mode, PISD was placed in the direction of the incoming beam of the blue laser diode having an excitation wavelength of 445 nm in such a way that the PISD reflected laser beam may not fall into the laser cavity, which may cause damage to the laser cavity. When the blue laser diode beam falls on yellow PISD, it generates white light peaking at 550 nm whose emission was collected simultaneously. The generated white light is an outcome of the mixture of two colors, one from the blue laser emission and other emission from yellow PISD; combination of these two produces highly efficient white light. The PISD shown in Figure 3b is used in this mode for the white light generation. It may be noted that the tunability of the laser power can control the intensity of the white light as well as the reflected light.

The schematic of transmission geometry is shown in **Figure 7**a. The optical geometry with the PL arrangement under normal and dark light is shown in Figure 7b,c, respectively. Figure 7d represents the PL emission spectrum of the blue diode laser. Figure 7e exhibits the in situ PL emission spectrum of white light produced from blue laser-excited PISD. Inset of Figure 7e represents the color coordinates of blue laser $X = 0.1288$, $Y = 0.0963$ (marked as A), yellow phosphor $X = 0.4488$, $Y = 0.5331$ (marked as B), and white light produced during the transmission mode $X = 0.3473$, $Y = 0.3140$ (marked as C), respectively. The color mixing of blue laser and yellow phosphor to produce white light is represented by a black line. In addition, we have taken the PL spectra of white light after every 2 h till 10 h to examine the photo stability of white light, and resultant spectra are shown in Figure 7f. It has been observed that there is no significant change in the PL spectrum after 10 h of continuous lighting as well as no thermal damage has been seen in PISD, confirming the thermal stability of PISD to the blue laser diode. The only drawback in the transmission mode is the high optical loss, as the phosphor emission is back-scattered toward the blue laser diode source. To address this issue, we strategically approached to design reflection mode geometry.

2.4.2. Reflection Mode

In the reflection mode, the optical assembly is analogous to that of the transmission mode, but the only difference is the reflecting mirror introduced in the geometry, which is placed in front of the blue laser at an optimized angle so that secondary intense blue laser beam is incident onto the PISD. The PISD with an aluminum-coated base is used in the reflections mode geometry, shown in Figure 3c. It is placed in the geometry in such a way that the transparent top surface must be exposed to the laser beam to produce white light, while the aluminum-coated surface kept at the back. The reason for using PISD with the aluminum-coated base is that the top sapphire disc protects the layer from

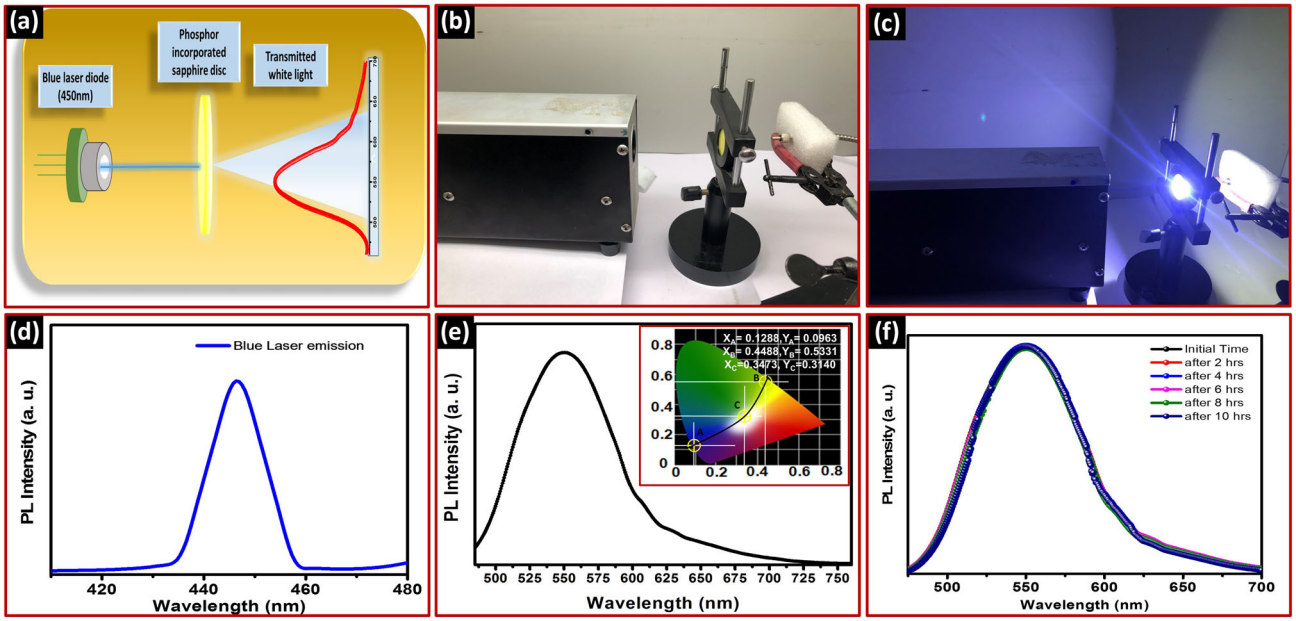

Figure 7. a) Schematic geometry of the transmission mode. b) Transmission mode geometry arrangement in normal light. c) Laser-induced white light in the transmission mode. d) PL spectrum of blue laser. e) PL spectrum of laser-induced white light through the transmission mode. f) Laser-induced white light spectrum at different hours in the transmission mode.

the thermal damage, whereas the aluminum-coated base acts as a heat sink as well as a reflecting substrate. The emitted white light is made focused by using a parabolic reflector and the incident laser beam is reflected back toward the reflecting mirror. The PISD and reflecting mirror are placed perpendicular to each other, so that the incident beam reflects back and forth between them and forms a cavity, which in addition increases the white light emission.

The schematic arrangement of the reflection mode is shown in **Figure 8**a. In the reflection mode, it was observed that by placing the reflecting mirror perpendicular to the PISD emits maximum amount of light on the parabolic reflector. Thus, this optical arrangement provides a better solution to obtain good efficiency of white light as multiple reflections takes place, and the addition of all the reflection results into the brighter white light. Figure 8b,c shows the optical geometry under day and dark light,

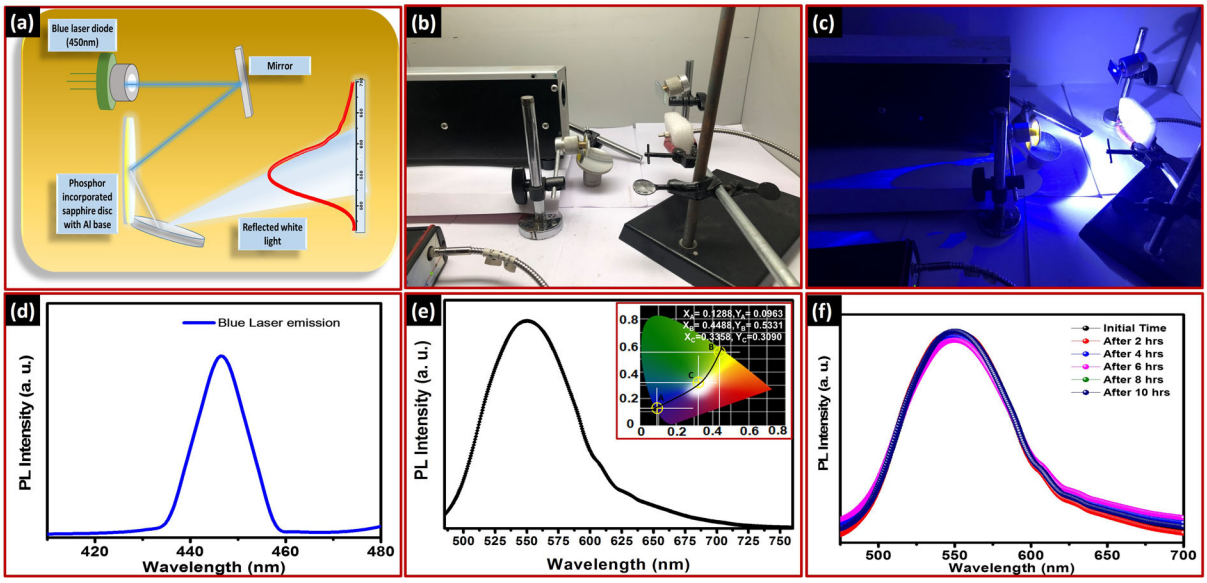

Figure 8. a) Schematic geometry of the reflection mode. b) Reflection mode geometry arrangement in normal light. c) Laser-induced white light in the reflection mode. d) PL spectrum of blue laser. e) PL spectrum of laser-induced white light through the reflection mode. f) Laser-induced white light spectrum at different hours in the reflection mode.

Table 1. Comparative study of luminous efficiency of commercially available CoB-based yellow phosphor-coated WLED arrays (LED flood light) outdoor display light, yellow phosphor synthesized in our laboratory, and coated on commercially available CoB-based blue LED arrays (LED flood light) outdoor display light, and laser-induced white light in transmission as well as reflection modes.

S. No.	Source	Power [W]	Luminous efficiency [lumen W^{-1}]
1	Commercially available CoB-based yellow phosphor-coated WLED arrays (LED flood light) outdoor display light	10	81.7
2	Yellow phosphor synthesized in our laboratory and coated on commercially available CoB-based blue LED arrays (LED flood light) outdoor display light	10	94.4
3	Laser-induced white light using PISD in the transmission mode	0.8	203.6
4	Laser-induced white light using PISD in the reflection mode	0.8	284.5

respectively. Simultaneously, the PL emission of the blue laser source of excitation and blue laser-induced white light has been taken in the reflective mode as shown in Figure 8d,e, respectively. The inset of Figure 8e represents the color coordinates of the blue laser $X = 0.1288$, $Y = 0.0963$ (marked as A), yellow phosphor $X = 0.4488$, $Y = 0.5331$ (marked as B), and white light $X = 0.3358$, $Y = 0.3090$ (marked as C), respectively. The color mixing of blue laser and yellow phosphor to produce white light is represented by black continuous line. To examine the photo stability of white light, the PL spectra of white light were taken after every 2 h for 10 h as shown in Figure 8f. No minor change was observed in the PL spectrum even after 10 h. In addition, the PL intensity of PISD is also measured for 3 days under different atmospheric seasons (15, 25, and 40 °C), as seen in Figure S4, Supporting Information. Thus, the result confirms the higher-efficiency and thermal stability of PISD. Furthermore, the white light generated in the reflection mode via the blue laser diode is compared with various white light generation sources under different setups, e.g., xenon lamp with 450 nm excitation wavelength, as-synthesized yellow phosphor coated chip on board (CoB)-based blue LED arrays (LED flood light) outdoor display light, commercially available CoB-based yellow phosphor-coated WLED arrays (LED flood light) outdoor display light, and their respective produced white light is shown in the Figure S5a–h, Supporting Information. It has been proved with the comparative study of the PL spectra of laser-induced white light using PISD, xenon lamp-induced white light using PISD, yellow phosphor synthesized in our laboratory coated on CoB-based blue LED arrays (LED flood light) outdoor display light induced white light, and commercially available CoB-based yellow phosphor coated WLED arrays (LED flood light) outdoor display light induced white light represented with black, red, pink, and blue curves, respectively are shown in Figure S6, Supporting Information, that the PL intensity of laser-induced white light using PISD enhanced manifold ($>10^3$) as compared with the intensity obtained with excitation with xenon lamp and ($>10^2$) as compared CoB-based LED sources. Moreover, we measured the brightness of blue laser (0.8 W)-induced highly efficient white light by using Konica Minolta LS-110 instrument shown in Figure S7, Supporting Information and converted the values into luminous efficiency for both reflection and transmission modes (**Table 1**). We have also measured the luminous efficiency of other light sources such as commercially available CoB-based yellow phosphor-coated WLED arrays (LED floodlight) outdoor display light induced white light having power of 10 W and yellow phosphor synthesized in our laboratory and coated on commercially available CoB-based blue LED arrays (LED flood light) outdoor display light induced white light are shown in Table 1. Finally, by analyzing all the sources, it has been found that the reflection mode provides a better solution for producing highly efficient white light through laser-induced PISD. In addition, the gradual increase in beam divergence in the reflection mode geometry also contributes to higher intensity for light with better uniformity. The major advantage of the reflection geometry is the added safety in any lighting application that in any eventuality, if the laser is not automatically switched off, there would be no damage to the end user whether it is on the road or otherwise. In a nutshell, the parabolic reflection geometry–based white light generation through laser-induced PISD could be the most promising solution, due to its compactness, simplicity, and efficiency. The unique optical geometry for such a lighting system proposed in the present work for the laser-assisted remote phosphor popularly known as laser assisted remote phosphor (LARP) would lead to revolutionize its automotive applications.[1–3]

3. Conclusion

In the present study, a successful facile, scalable, and inexpensive synthesis method for $Y_{2.82}Al_5O_{12}$:0.18 Ce^{3+} phosphor to design the PISD for producing highly efficient white light through transmission and reflection modes is presented. The strategical design of the PISD provides a light weight, compact, thermally stable geometry to produce highly efficient white light. Furthermore, the white light intensity emitted by the designed PISD under the excitation wavelength of 445 nm, via, blue laser diode gets augmented by several orders of higher magnitude than the intensity when it is excited by 450 nm wavelength of xenon lamp. The experimental demonstration of two different modes of geometries, i.e., transmission and reflection suggests that the reflection mode could be a better geometry that provides a better heat sink facility and also protects PISD from the intense beam of blue laser, simultaneously, also gives a large beam of divergence, which makes it safer, suitable, and efficient for automotive applications. Thus, the reflection mode might be a legitimate geometry for automotive industries to design more compact and light weighted headlights using PISD to produce highly efficient white light as compared with other conventional white light sources.

4. Experimental Section

Raw Materials: Y_2O_3 (99.99%), $Ce(NO_3)_3.6H_2O$(99.99%) as rare-earth sources, whereas for Al, $Al(NO_3)_3.9H_2O$ (99.99%), nitric acid (HNO_3), urea $CO(NH_2)_2$ were used as precursors. All chemically pure reagents

used in the synthesis of nanocrystalline powder of YAG:Ce by auto-combustion process were of analytical (AR) grade and used as received without further purification. Deionized water was used throughout the experiments.

Preparation of Phosphor Powder: The yellow powder of $Y_{3-x}Al_5O_{12}:xCe^{3+}$ ($0.03 \leq x \leq 0.24$) was synthesized by a facile customized auto-combustion process with the aforementioned precursor materials as compared with our previously reported results for WLEDs applications.[22] Here, a customized auto-combustion process was employed to control the oxygen environment in a box furnace to avoid the additional use of boric acid. In addition to this, the initial heating steps were modified, during the conversion of gel into spumous powder before doing its calcinations at a high temperature (1400 °C) in the box furnace. In our earlier studies, the nitrate precursor (thick gel) was heated on an electric coil heater to convert it into the spumous form. However, in the present study, the nitrate precursor (thick gel) was heated in the box furnace to avoid the uneven heating of the nitrate precursor through an electric coil. The major advantage of this process is that in a muffle box furnace, the heating was uniform in controlled air atmosphere that helps the organic fuel (urea; $CO(NH_2)_2$) to ignite fire uniformly during the auto-combustion process without leaving any residue of urea behind. As an outcome of this process, the high yield synthesis of the spumous powder was obtained without mass loss as in the previous process due to uneven heating. Even no flux was required during the calcination process of the spumous powder, due to controlled oxygen environment in a muffle furnace. For the synthesis of $Y_{3-x}Al_5O_{12}:xCe^{3+}$ ($0.03 \leq x \leq 0.24$), a stoichiometric amount of yttrium oxide Y_2O_3 was dissolved in a hot solution of 15 mL de-ionised (DI) water and 5 mL nitric acid in a beaker followed by an uninterrupted stirring at a temperature of 70–75 °C until Y_2O_3 got completely dissolved to form a clear solution of yttrium nitrate. Afterward, aluminum nitrate and cerium nitrate were added one by one in a beaker, which gives a bright yellow color to the solution with continuous stirring and heating at a temperature of 120–125 °C, to evaporate the excessive amount of nitric acid. Then, the reduced solution was immersed in a water bath to obtain the gel. Subsequently, urea was added to the gel by the ratio of half the mole of the total metal ions. The quantity of urea plays a vital role in the redox reaction, i.e., if there was inadequate urea then Ce ions would not be reduced fully into Ce^{3+}. On the other hand, too much of urea would decrease the luminescence steadily. The redox reaction for the synthesis of YAG is shown in Equation (4)

$$3Y(NO_3)_3 + 5Al(NO_3)_3 \cdot 9H_2O + 20\,NH_2 \cdot CONH_2 \rightarrow Y_3Al_5O_{12} + 32\,N_2 + 49\,H_2O + 20\,CO_2 \quad (5)$$

where oxygen from metal nitrates acts as oxidizing agent while C, H and Y act as reducing agents. There was no significant role of nitrogen in the combustion reaction nor did it act as oxidizer or as reducer. The mixing of metal nitrates and organic fuel (urea) in the gel maximize the atomic mixing of the elements. After mixing the organic fuel, on further heating, the gel get thickened and the canary xerogel was obtained. Then, the obtained xerogel was put into a muffle furnace which was pre heated at 400 °C for 20 min where the auto-combustion reaction took place. The auto-combustion's exothermic reaction resulted in the formation of pale yellow spumous powder of YAG:Ce. This pale yellow spumous powder of YAG:Ce was further kept in the box furnace and calcined at a high temperature (1400 °C) with the rate of 10 °C min^{-1} for 2 h to achieve the homogeneous YAG phase. After the calcination process, a bright yellow color YAG:Ce powder was obtained. The calcination temperature and time were optimized after several runs. The optimization of temperature and time is necessary to avoid any kind of secondary phase.[10]

Preparation of PISD: An appropriate ratio of the epoxy resin and phosphor was taken to disperse the as-synthesized yellow phosphor uniformly in the epoxy resin using a solvent exchange process. Primarily, for the fabrication of single disc, ≈0.5 mg of phosphor was dispersed in 2 mL epoxy solution, where the epoxy solution comprised the mixture of epoxy resin and the hardening agent, i.e., triethylene tetra amine in the ratio of 100:12.5 by volume. The solution was mixed evenly to make a homogenous mixture. Simultaneously, the transparent sapphire discs were heated at 80 °C temperature to provide a good adhesion between the disc and the phosphor layer. Afterward, the prepared homogenous mixture solution was poured over the heated sapphire disc slowly and carefully so that the mixture did not spill out of the disc. Later, it was left undisturbed for 24 h at room temperature to get settled down and simultaneously, it will get hard. The schematic of fabrication of PISD by integrating the homogenous mixture of phosphor in epoxy on the sapphire disc is shown in Figure 3a.

Characterization: To study the crystalline structure of the sample, X-ray powder diffraction was done by using Bruker AXS D8 Advance X-ray diffractometer, using Cu $K\alpha_1$ radiation ($\lambda = 1.5406$ Å). Carl ZEISS EVO 18 scanning electron microscope (SEM) was used to investigate the surface morphologies of the samples, along with that elemental analysis of samples were carried out by EDAX attachment with the SEM system. Edinburgh spectrometer was used to measure the PL and TRPL of as-synthesized YAG:Ce phosphor powder, where a xenon lamp and microsecond flash lamp, respectively, were used as the source of excitation. The internal quantum yield of as-synthesized as well as commercial phosphors was estimated using an Edinburgh spectrometer (model F900) instrument equipped with an integrating sphere. The PL spectrum of PISD has been recorded using AvaSpec-ULS2048 star line versatile fiber-optic spectrometer of Avantes, where blue laser of 445 nm wavelength acts as an excitation source. The luminous efficiency has been measured by using Konica Minolta LS-110 make luminance meter. For the comparative studies, CoB-based blue LED arrays (LED flood light outdoor display light; 10 W power, 120° beaming angle, DC 12 V, InGaN-based ROHS, an ISO 9001 registered company, made in China) was used. Microtroniks Chemical Mercury Thermometer (−10 to 360 °C) was used for temperature measurements.

Supporting Information

Supporting Information is available from the Wiley Online Library or from the author.

Acknowledgements

The authors thank Dr. D. K. Aswal, Director, N.P.L., New Delhi, for his keen interest in the consultancy project of CSIR-NPL on "Development of YAG:Ce yellow phosphor integrated with blue diode laser to produce white light for a car headlight applications" from Fiem Industries Ltd., Sonepat-131029, Haryana, India. The authors are thankful to Prof. S. K. Joshi (CSIR-NPL) and Prof. O. N. Srivastava (Banaras Hindu University, Varanasi) for his encouragement. The authors (NPL Team) gratefully acknowledge the National Post Doctoral Fellowship (N-PDF-PDF/2017/002479), Department of Science and Technology, Govt. of India, and Council of Scientific and Industrial Research (CSIR), Government of India for financial assistance to carry out this work [CSIR-SRF, Award No. 31/01(0508)/2018-EMR-I].

Conflict of Interest

The authors declare no conflict of interest.

Keywords

blue laser diodes, optical geometry, photoluminescence, white light conversion, yellow phosphor

Received: February 11, 2019
Revised: May 24, 2019
Published online: July 22, 2019

[1] Y. Nanushi, *Nat. Photonics* **2014**, *8*, 884.
[2] V. Bachmann, C. Ronda, A. Meijerink, *Chem. Mater.* **2009**, *21*, 2077.
[3] A. Aboulaich, M. Michalska, R. Schneider, A. Potdevin, J. Deschamps, R. Deloncle, G. Chadeyron, R. Mahiou, *ACS Appl. Mater. Interfaces* **2014**, *6*, 252.
[4] H. Daicho, T. Iwasaki, K. Enomoto, Y. Sasaki, Y. Maeno, Y. Shinomiya, S. Aoyagi, E. Nishibori, M. Sakata, H. Sawa, S. Matsuishi, H. Hosono, *Nat. Commun.* **2012**, *3*, 1.
[5] S. Pimputkar, J. S. Speck, S. P. DenBaars, N. Shuji, *Nat. Photonics* **2009**, *3*, 180.
[6] D. A. Steigerwald, J. C. Bhat, D. Collins, R. M. Fletcher, M. O. Holcomb, M. J. Ludowise, P. S. Martin, S. L. Rudaz, *IEEE J. Sel. Top. Quantum Electron* **2002**, *8*, 310.
[7] K. Toshihiko, N. Masao, *IEEE Trans. Consum. Electron* **2004**, *50*, 100.
[8] Z. Xia, A. Meijerink, *Chem. Soc. Rev.* **2017**, *46*, 275.
[9] H. Chen, H. Lin, J. Xu, B. Wang, Z. Lin, J. Zhou, Y. Wang, *J. Mater. Chem. C* **2015**, *3*, 8080.
[10] D. N. Chung, D. N. Hieu, T. T. Thao, V. V. Troung, N. N. Dinh, *J. Nanomater.* **2014**, 571920.
[11] P. Pust, P. J. Schmidt, W. Schnick, *Nat. Mater.* **2015**, *14*, 454.
[12] N. Trivellin, M. Yushchenko, M. Buffolo, C. D. Santi, M. Meneghini, G. Meneghesso, E. Zanoni, *Materials* **2017**, *10*, 1166.
[13] Y. H. Song, E. Kyung, B. W. Jeong, M. K. Jung, E. Y. Kim, D. H. Yoon, *Sci. Rep.* **2016**, *6*, 31206.
[14] B. Reiss, J. Ripperger, *Auto Tech Rev.* **2018**, *7*, 32.
[15] B. K. Gupta, D. Haranath, S. Saini, V. N. Singh, V. Shanker, *Nanotechnology* **2010**, *21*, 055607.
[16] B. K. Gupta, V. Rathee, T. N. Narayanan, P. Thanikaivelan, A. Saha, S. P. Singh Govind, V. Shanker, A. A. Marti, P. M. Ajayan, *Small* **2011**, *7*, 1767.
[17] Y. Pan, M. Wu, Q. Su, *J. Phys. Chem. Solids* **2004**, *65*, 845.
[18] R. Kasuya, T. Isobe, H. Kuma, *J. Alloys Compd.* **2006**, *9*, 820.
[19] S. Murai, K. Fujita, K. Iwata, K. Tanaka, *Opt. Mater.* **2010**, *33*, 123.
[20] J. D. Furman, G. Gundiah, K. Page, N. Pizarro, A. K. Cheetham, *Chem. Phys. Lett.* **2008**, *465*, 67.
[21] Sapphire Physical and Mechanical Properties, https://www.cmscientific.com/info_sheets/Sapphire_Physical_Mechanical_Properties.pdf.
[22] J. Dwivedi, P. Kumar, A. Kumar, Sudama, V. N. Singh, B. P. Singh, S. K. Dhawan, V. Shanker, B. K. Gupta, *RSC Adv.* **2014**, *4*, 54936.